Electron Beam Lithography on Irregular Surfaces Using an Evaporated Resist

Jian Zhang, Celal Con, and Bo Cui*

Department of Electrical and Computer Engineering and Waterloo Institute for Nanotechnology (WIN), University of Waterloo, Waterloo, Ontario N2L 3G1, Canada

ABSTRACT An electron beam resist is typically applied by spin-coating, which cannot be reliably applied on nonplanar, irregular, or fragile substrates. Here we demonstrate that the popular negative electron beam resist polystyrene can be coated by thermal evaporation. A high resolution of 30 nm half-pitch was achieved using the evaporated resist. As a proof of concept of patterning on irregular surfaces, we fabricated nanostructures on the AFM cantilever and the optical fiber. Although an ice (H_2O) resist has also been recently demonstrated as being capable of nanopatterning on irregular and fragile substrates, it requires specially designed accessories mounted inside a SEM chamber, whereas our process works with any thermal evaporator and is thus simpler and much more accessible. Nanofabrication on nonplanar surfaces may find applications in fields such as (AFM) tip-enhanced Raman spectroscopy for chemical analysis and lab-on-fiber technology.

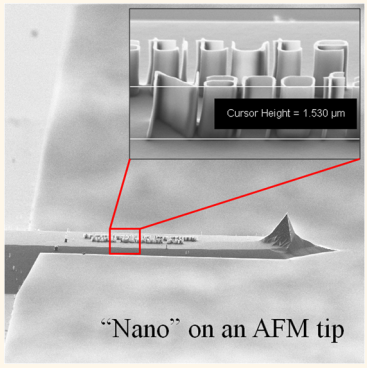

KEYWORDS: electron beam lithography · resist · polystyrene · evaporation

One challenge in nanofabrication is to pattern on nonflat or prestructured surfaces, which is desired in many fields such as MEMS,[1] electronic devices,[2] superadhesive surfaces,[3] and optical devices.[4] For example, nanopatterning on optical fibers allows the so-called lab-on-fiber technology,[5] and that on an atomic force microscope (AFM) tip allows tip-enhanced Raman spectroscopy,[6] near-field optical focusing,[7,8] and the study of fundamental quantum mechanical systems.[9,10] In addition, nanofabrication on a cylindrical roller may be needed as the mold for roll-to-roll nanoimprint lithography (NIL).[11,12] However, it is far more challenging to fabricate nanostructures on nonflat surfaces than flat ones such as a wafer, for which the popular resist coating method spin-coating works well.

Previously, various methods have been demonstrated to create nanostructures on nonflat surfaces. For slightly nonflat yet regular surfaces such as a macroscale curved surface, spin-coating may still be employed to coat the resist, which can be patterned by NIL using a flexible mold capable of conformal contact to the surface.[13] For a nonplanar surface without sharp corners or edges such as a V-shaped trench on a wafer, spray coating may be used to coat a uniform layer of resist over the trench.[14] Spin-coating using a very low viscosity resist solution can be coated uniformly on the side of ridges patterned on a silicon wafer, yet only when the ridge is aligned along the radial direction during spinning.[15] Electron beam resist applied by the Langmuir–Blodgett method can also be coated on a curved surface, but pattern transfer by dry etching is problematic due to the extremely thin resist thickness;[16] this is also the case for a self-assembled monolayer resist (pattern transfer through an intermediate wet etching step has been demonstrated, yet wet etching has poor CD control compared to dry etching).[17,18] In principle, the resistless nanolithography method, notably focused ion beam milling or deposition, can be used to pattern any surface, yet its cost is higher and its throughput is much lower than electron beam lithography (EBL). Therefore, we believe EBL using a vacuum-deposited resist is the most efficient method for patterning irregular nonplanar surfaces.

Previously, Pedersen *et al.* have reported the coating of an electron beam resist using plasma-polymerized hexane.[19] The resulting hydrocarbon resist presented a negative tone when developed in a 1:1 mixture of cyclopentanone and *o*-xylene for 40 min. However, besides its low sensitivity and

* Address correspondence to bcui@uwaterloo.ca.

Received for review December 17, 2013 and accepted March 26, 2014.

Published online March 26, 2014
10.1021/nn4064659

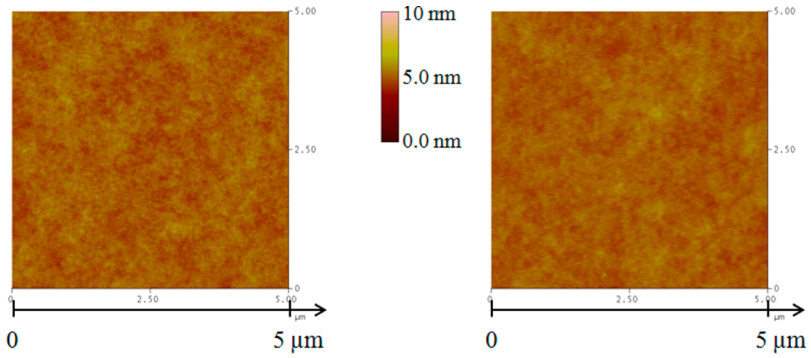

Figure 1. AFM images of PS films prepared by the spin-coating method (left) and thermal evaporation (right).

poor resolution (demonstrated a 150 nm wide sparse line array), this approach is not ideal for a wide range of applications, as it needs a special custom-built plasma chamber. Eric *et al*. have developed a negative evaporated sterol resist, named QSR-5, which was employed to pattern on an optical fiber and laser diode facet, as well as on the backside of membranes for the fabrication of an X-ray mask.[20−22] Yet, in addition to its moderate resolution, this specially formulated resist is not commercially available. Daniel *et al*. introduced water vapor into the SEM chamber and formed ice on an AFM cantilever or graphene film, which was cooled to <120 K. The thin ice layer was patterned by e-beam exposure with low voltage. This novel patterning process is named ice lithography.[6,23,24] However, for ice lithography the resist has to be kept at very low temperature before pattern transfer by liftoff or dry etching is completed, thus a specially designed tool or tool accessory is needed. In addition, the resist sensitivity is very low, three orders lower than PMMA, which is already considered an insensitive resist. Similar to ice, frozen CO_2 can also be used as an electron beam resist, although it would suffer from the same drawbacks as an ice resist.[25] A metal halide such as AlF_3 is another type of inorganic evaporated resist, which again suffers from extremely low sensitivity, and it is able to form only line or dot (not areal) patterns.[26,27] Lastly, silicon dioxide, which can be grown or coated by various thin film deposition methods, has been used as a kind of electron beam resist, yet its sensitivity is again extremely low.[28]

Therefore, there is still a great demand for a simple process using a cheap and readily available evaporative resist for nanofabrication by EBL on an irregular nonflat surface with high resolution. Here we will show that low molecular weight polystyrene (PS) satisfies all these criteria. Although its sensitivity is much lower than PMMA, it is two orders higher than the above-mentioned inorganic resists (*e.g.*, >1 C/cm^2 needed for exposing an ice resist). Previously we have demonstrated that PS is a very versatile negative resist, offering an ultrahigh resolution of a 15 nm period dense dot array pattern for low molecular weight[29] and very high sensitivity on the order of 1 μC/cm^2 at

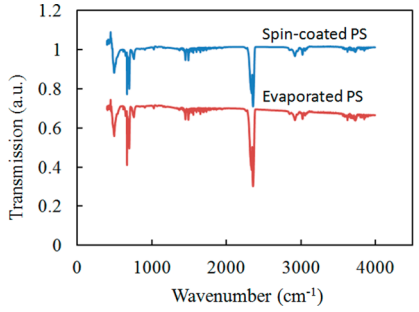

Figure 2. FTIR spectra of PS films coated on a KBr substrate by spin-coating and thermal evaporation methods. The spectra were shifted relative to each other along the vertical axis for clarity.

5 keV for high molecular weight.[30] Its dry etching rate is much lower than that of PMMA, which is a desirable property for pattern transfer using plasma etching. Moreover, it can be dry thermally developed to reduce pattern collapse due to the capillary force when using solvent development.[31] Additional advantages for an evaporated resist over spin-coating include the lack of edge bead effect, which is a serious issue for spin-coating on small samples such as a single-crystal diamond,[32] precise control of film thickness, uniform coating around dust particles on substrates, and negligible attack to the substrate material, which may be a polymer susceptible to dissolution or swelling by the solvent used for spin-coating.

RESULTS AND DISCUSSION

Figure 1 shows the AFM images for an evaporated and spin-coated PS film. As can be seen, the roughness of the two films was very close to each other, with a mean roughness (Ra) of 0.239 and 0.223 nm for the spin-coated and evaporated film, respectively. However, although not evident in the AFM images, for a spin-coated film the uniformity is also affected by the dust on the substrate and the edge bead effect. The IR transmission spectra for the PS film prepared by thermal evaporation and the spin-coating method are shown in Figure 2. Both the spectra of evaporated and spin-coated PS show peaks at 2700−3200 (attributed

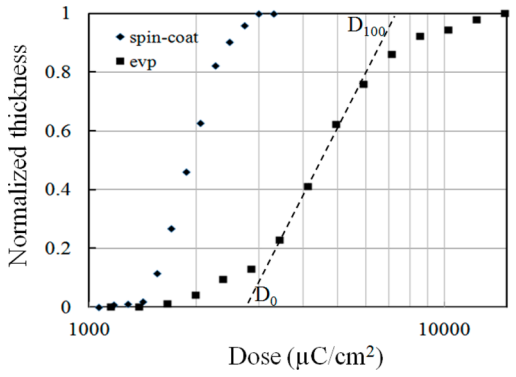

Figure 3. Contrast curves for 1.2 kg/mol polystyrene by spin-coating and thermal evaporation. Both were exposed at 5 keV and developed by xylene. The sensitivity (dose for 50% remaining thickness) and contrast are 1920 μC/cm^2 and 4.3 for spin-coated PS and 4500 μC/cm^2 and 2.6 for evaporated PS.

to the ═CH− group), 1500, 1450, 1020 (attributed to the aromatic group), and ~500 cm^{-1} (attributed to the −CH_2− group). This suggests that the PS film coated by evaporation was not modified chemically during heating and can thus be employed as an electron beam resist the same way as a spin-coated film.

Figure 3 shows the contrast curves for the PS coated by spin-coating and evaporation. The contrast of evaporated PS exposed at 5 keV, defined as $\gamma = [\log(D_{100}/D_0)]^{-1}$, is calculated to be 2.6, and the sensitivity (D_{50}) was derived as 4500 μC/cm^2. The contrast of the spin-coated PS is 4.3 with a sensitivity of 1920 μC/cm^2. As seen, the sensitivity is lower for evaporated polystyrene, which indicates the evaporated film has a lower molecular weight due to partial decomposition during evaporation. In fact, we believe that PS can be thermally evaporated because its thermal decomposition involves not only end-chain scission (unzipping process), which gives styrene monomer, which cannot form a solid film, but also random chain scission, which leads to a PS chain with reduced molecular weight and increased volatility to form the film on the substrate surface.[33] On the contrary, the other popular electron beam resist PMMA cannot be thermally evaporated since its thermal decomposition is mainly an unzipping process. For other polymer resists such as polycarbonate,[34] the thermal decomposition is not by chain scission, but by significant chemical structure modification (generating carbon dioxide, bisphenol A, and phenol for polycarbonate, leaving behind a char); thus they are unsuitable for coating by thermal evaporation.

To study the resolution capability of the polystyrene resist, we exposed periodic dense line arrays with periods down to 40 nm at 5 keV. The line was written by single-pass exposure with a step size of 6 nm. Figure 4 shows line array patterns of 50 and 60 nm periods, which are both well-defined. A line array with a smaller period was found collapsed because of the

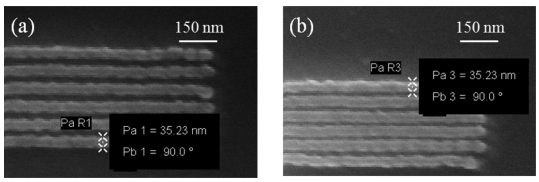

Figure 4. Line array patterns with 60 nm (a) and 50 nm period (b) exposed at a line dose of 18.4 nC/cm.

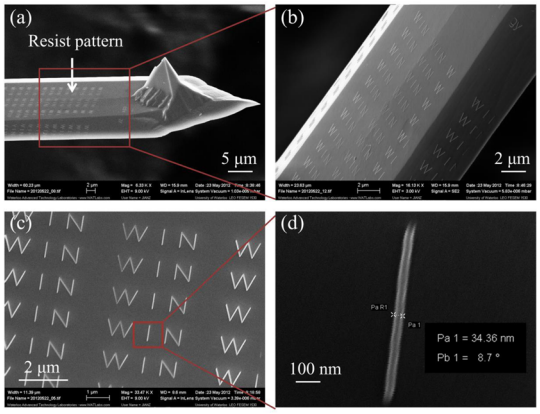

Figure 5. SEM images of patterned PS on an AFM cantilever by EBL, taken at increasing magnifications from (a) to (d). The exposed pattern is "WIN", standing for Waterloo Institute for Nanotechnology.

capillary force during the drying of the rinsing liquid. The obtained half-pitch of 50 nm is much smaller than the previously reported evaporated resists.[19−22] To demonstrate its patterning capability on a nonflat surface, 50 nm PS film was evaporated onto an AFM cantilever and exposed with the same conditions. An array of letters "WIN" (Waterloo Institute for Nanotechnology) with a line width of 34 nm was successfully patterned on an AFM cantilever, as seen in Figure 5.

For most applications it is desirable to transfer the pattern from the resist to the sublayer or substrate. As a proof of concept, we fabricated a metal (here Al-coated sputtering) pattern by reactive ion etching (RIE) with BCl_3 gas using the resist as mask, and if desired, the pattern can be further transferred into the underlying silicon using Al as a hard mask. The pattern in Al and silicon is shown in Figure 6. The starline pattern in Figure 6a demonstrated the exposure uniformity along all directions. Figure 6b shows the Al "circuit" pattern with a line width of about 60 nm, which was transferred to the Si substrate with a depth of 200 nm, as shown in Figure 6c. A high-aspect-ratio (1:20) pattern of the name of our Institute and Group (Waterloo Nanofabrication Group) was achieved by a longer etching time to give a pattern height of 2 μm, as shown in Figure 6d.

Recently, nanofabrication on an optical fiber has attracted growing attention in various aspects, such as applications in Bragg gratings,[35] optical filters,[36,37] SERS sensors,[38,39] plasmonic lens,[40,41] and transmission measurement.[42,43] Our process using an evaporated resist can be equally applied to patterning an

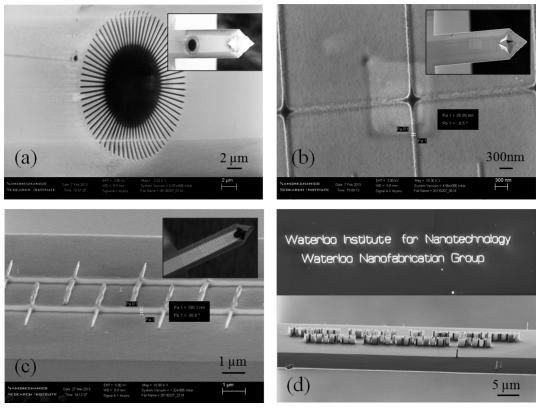

Figure 6. SEM images of (a) Al starline pattern, which demonstrated the exposure uniformity along all directions. (b) Al "circuit" pattern with a line width of about 60 nm. (c) Same pattern as (b), after pattern transfer into Si by 1 min RIE for a pattern height of 200 nm. (d) High-aspect-ratio (1:20) pattern of the name of our Institute and Group by 10 min RIE for a pattern height of 2 μm.

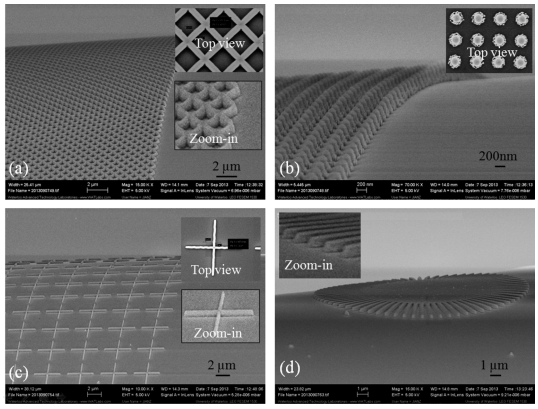

Figure 7. SEM images of nanostructures on an optical fiber with a height/depth of 270 nm. (a) 2D grating array with a line width of 167 nm; (b) dot array with a diameter of 200 nm; (c) crossbar array with a line width of 167 nm; and (d) starline pattern. The insets show a top view and/or zoom-in view of the structures. The insets show a top view (pattern on the top surface) and/or zoom-in view of the structures. Except for the top-view images, the wafer piece onto which the fiber was attached was mounted on a 45°-tilted stub for SEM imaging.

optical fiber, as shown in Figure 7. Evaporated PS on a fiber (cladding layer removed) was exposed by EBL; then the patterns were transferred to an Al layer and fiber (SiO_2) by BCl_3 RIE followed by CF_4 RIE for high-aspect-ratio structures. Figure 7a shows the tilted SEM image of the two-dimensional grating array after CF_4 RIE. With the patterned Al structure as an etching mask, a pattern on fiber having a depth of 270 nm was achieved. Figure 7b,c show a dot array with a diameter of 200 nm and a crossbar array with a line width of 167 nm, both etched into the fiber for 270 nm, respectively. To demonstrate the uniformity along different directions, a starline pattern was exposed and etched into the fiber as shown in Figure 7d. Figure 8 compares the 2D grating pattern (same sample as Figure 7a) on the top and side surface of the fiber. To image the pattern on the top surface, the fiber was mounted on a normal stub, whereas to image the pattern on the side surface (here $\theta = 70°$ away from the top), the fiber was mounted on a 70°-tilted stub. As expected, the pattern on the top surface (Figure 8a) is well-defined. The pattern on the side surface (Figure 8b) has a 70° electron beam incidence angle during exposure; thus the structure is tilted by the same angle. We have previously achieved a similar tilted structure by exposing a wafer mounted on a tilted stub.[44] Moreover, the cross sections of two orthogonal lines are taller than the line sections next to them. This is because the exposure dose is reduced to cos 70° = 0.34 × nominal line dose, and thus the lines were greatly underexposed, which led to a shorter resist structure after development. However, the cross sections received twice the exposure, which gave taller resist structures sufficient for the subsequent pattern transfer process. The underexposure at large angle can be compensated through increasing the dose by 1/cos θ. The 2D grating pattern eventually disappeared

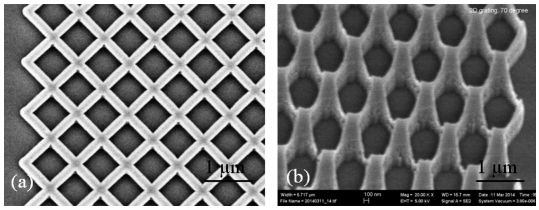

Figure 8. SEM images of the 2D grating pattern on a fiber. (a) Perpendicular nanostructure on the top surface ($\theta = 0°$); (b) tilted nanostructure on the side surface ($\theta = 70°$). Note that for (b) the fiber support was mounted on a 70°-tilted stub, and thus the electron beam had normal incidence during SEM imaging.

when θ is too large, which led to too low exposure dose and/or too thin resist film (both dose and thickness are proportional to cos θ if without dose compensation).

For evaporation on a curved surface of an optical fiber, one consequence of the nonuniform resist thickness is related to the resist sensitivity. For a given development time, positive/negative resist sensitivity increases/decreases with reduced film thickness. Therefore, for a nominal exposure dose varying by 1/cos θ (to maintain the same areal dose along the side surface), when the negative resist on the top ($\theta = 0°$) of the fiber is properly exposed, the resist on the side would be underexposed or overdeveloped since it is thinner. The degree of underexposure/over-development and the resulting feature size shrinkage strongly depend on the resist contrast. For a resist with reasonably high contrast, such as low M_w polystyrene, the overdevelopment would not cause significant feature size shrinkage because the lateral development toward the more exposed region is very slow.

Unlike an AFM cantilever that has a flat top surface, the side surface of an optical fiber has a circular shape.

Thus, the electron beam will be out of focus and distorted away from the top of the fiber surface, where the beam was well focused with minimal stigmation. As a consequence, the achievable resolution on the fiber side surface depends heavily on the depth of focus (DOF) of the electron beam. We can ignore the wave nature and diffraction of the electron beam when the feature size is well above 10 nm, as is the case for the current work. Then DOF is inversely proportional to the aperture size and proportional to the working distance. A large DOF can be obtained by using a small aperture size such as 7.5 μm, which is the smallest one for the Raith 150^{TWO} system, or using a large working distance such as 20 mm, which is the maximum for the system. However, a small aperture results in a long exposure time because the beam current is roughly proportional to the square of the aperture size, whereas a large working distance makes the exposure more susceptible to electromagnetic and vibrational noise. Therefore, a trade-off between exposure time and achievable resolution on the fiber side surface has to be made. For example, with 37 μm out of focus (fiber radius is 50 μm) and 30 μm aperture size, one can achieve 80 nm resolution on a flat wafer.[45] Moreover, in addition to beam enlargement (here to 80 nm diameter) due to out of focus, the beam spot size on the side surface is further elongated by 1/cos θ (θ is the local incident angle) along the vertical direction.

In addition to DOF, another two important factors for patterning on the side surface of an optical fiber are film deposition and dry etching uniformity. The film thickness for vacuum evaporation is proportional to cos θ, with θ being the incident angle, which is 0° for the top (horizontal surface) of the optical fiber and 90° for the vertical surface. To achieve a more uniform film, one can either continuously and automatically rotate the fiber along its axis during deposition or carry out multiple (*e.g.*, three times) depositions each time the fiber is mounted at a rotated angle (*e.g.*, 60°). As for the etching uniformity, it is less of a concern because, for dry plasma etching, the etching direction tends to be perpendicular to the local surface with similar ion energy and isotropic diffusion of free radicals to the local surface, which results in a weak dependence of the etching rate on the incident angle. As a matter of fact, one has to use a Faraday cage[46] or ion sheath control plate[47] in order to etch a tilted (*i.e.*, not normal to the wafer surface) nanostructure, because the self-formed electrical field inside a plasma environment, which determines the ion bombardment and thus the etching direction, is always perpendicular to the sample surface whether the sample is tilted or not.

CONCLUSION

We demonstrated here that polystyrene can be thermally evaporated and applied as an electron beam resist on a nonflat, irregular, or fragile substrate. Slight thermal decomposition occurred during evaporation, leading to a reduced molecular weight for the evaporated polystyrene and thus lower sensitivity as compared to the source material. A high resolution of 25 nm half-pitch was achieved using the evaporated resist. There are great potential applications of this coating technique in nanostructure and device fabrication. As a proof of concept of patterning on irregular surfaces, we fabricated nanostructures on the AFM cantilever and the optical fiber.

METHODS

We chose a low molecular weight of 1.2 kg/mol (Scientific Polymer Products Inc., Ontario, NY, USA) for PS thermal evaporation with a chamber background vacuum of 2 μTorr using an Intlvac vacuum deposition system. During the deposition, the heating power was increased slowly until a desired deposition rate of ~1 Å/s was achieved. The actual temperature of the heating boat containing PS powder was not monitored by the system, but is expected to exceed 575 K, at which appreciable weight loss was observed.[33] We were unable to obtain a uniform and thick-enough PS film for higher molecular weights such as 5 kg/mol because the process was unstable at the power needed to give significant vaporization. This process instability is due to the fast decomposition at higher temperatures and is in agreement with the observed initial sharp decrease in molecular weight when PS was gradually heated.[33]

The surface roughness of the PS films prepared by evaporation and spin-coating on silicon wafers was mapped by AFM. To examine the structural change of PS before and after thermal evaporation, we coated PS films by thermal evaporation and spin-coating on a KBr substrate and recorded their respective infrared transmission spectra using a Fourier transform infrared (FTIR) spectrometer (Bruker Vector-27, Bruker AXS GmbH, Karlsruhe, Germany). In addition, the decomposition of PS due to the high-temperature process can be examined indirectly by comparing its sensitivity with the spin-coated film, as it is known that for a simple cross-linking resist such as polystyrene the sensitivity (μC/cm^2) is inversely proportional to molecular weight (kg/mol).[48] Here for spin-coating, polystyrene powder with the same molecular weight of 1.2 kg/mol was dissolved in chlorobenzene with a concentration of 1.3 wt/vol %, which gave a film thickness of 140 nm. After spin coating, the film was baked at 90 °C for 5 min on a hot plate.

Electron beam lithography was conducted using a Raith 150^{TWO} system with 5 kV acceleration voltage and 0.2 nA beam current. The exposed PS was developed by xylene (mixture of *o*-, *m*-, and *p*-xylene) for 1 min and observed by LEO 1530 FE-SEM. Other solvents that can dissolve the unexposed PS, including chlorobenzene, toluene, anisole, and cyclohexane, can also be used as a PS developer with similar results. The PS film was typically 100 nm thick and was coated on low-resistivity (0.01−0.02 Ω·cm) silicon wafer pieces. An AFM cantilever and optical fiber were used to demonstrate its capability of patterning on nonflat surfaces. To prepare the surface for PS coating, the buffer layer of the fiber was removed by soaking in acetone and scrubbing, followed by a solvent cleaning using acetone and 2-proponol and a short exposure to oxygen plasma. For pattern transfer to the substrate using reactive ion etching, a hard RIE mask layer of 10 nm aluminum was coated by sputter deposition, which gives a better conformal coating on the irregular surfaces than vacuum deposition. After EBL and

development, the pattern was first transferred into the Al layer using ICP-RIE (Oxford Instruments ICP380 dry etching system, 50 sccm BCl_3, 5 mTorr, ICP power 800 W, RF bias power 200 W, 15 s) with the resist as a mask with the etching selectivity PS:Al = 2:1, then into the substrate with the patterned Al as hard mask using F-based gases that etch Si (for the AFM cantilever) and SiO_2 (for the optical fiber).

Conflict of Interest: The authors declare no competing financial interest.

Acknowledgment. This work was carried out using the nanofabrication facility at Quantum NanoFab funded by the Canada Foundation for Innovation, the Ontario Ministry of Research & Innovation, and Industry Canada. C.C. acknowledges the Ministry of Turkish National Education for financially supporting his study.

REFERENCES AND NOTES

1. Xia, Y. N.; Whitesides, G. M. Soft Lithography. *Annu. Rev. Mater. Sci.* **1998**, *28*, 153–184.
2. Ko, H. C.; Stoykovich, M. P.; Song, J. Z.; Malyarchuk, V.; Choi, W. M.; Yu, C. J.; Geddes, J. B.; Xiao, J. L.; Wang, S. D.; Huang, Y. G.; *et al*. A Hemispherical Electronic Eye Camera Based on Compressible Silicon Optoelectronics. *Nature* **2008**, *454*, 748–753.
3. Murphy, M. P.; Kim, S.; Sitti, M. Enhanced Adhesion by Gecko-Inspired Hierarchical Fibrillar Adhesives. *ACS Appl. Mater. Interface* **2009**, *1*, 849–855.
4. Zamarreno, C. R.; Matias, I. R.; Arregui, F. J. Nanofabrication Techniques Applied to the Development of Novel Optical Fiber Sensors Based on Nanostructured Coatings. *IEEE Sens. J.* **2012**, *12*, 2699–2710.
5. Consales, M.; Ricciardi, A.; Crescitelli, A.; Esposito, E.; Cutolo, A.; Cusano, A. Lab-on-Fiber Technology: Toward Multifunctional Optical Nanoprobes. *ACS Nano* **2012**, *6*, 3163–3170.
6. Han, A.; Kuan, A.; Golovchenko, J.; Branton, D. Nanopatterning on Nonplanar and Fragile Substrates with Ice Resists. *Nano Lett.* **2012**, *12*, 1018–1021.
7. Johnson, T. W.; Lapin, Z. J.; Beams, R.; Lindquist, N. C.; Rodrigo, S. G.; Novotny, L.; Oh, S.-H. Highly Reproducible Near-Field Optical Imaging with Sub-20-nm Resolution Based on Template-Stripped Gold Pyramids. *ACS Nano* **2012**, *6*, 9168–9174.
8. Lindquist, N. C.; Nagpal, P.; Lesuffleur, A.; Norris, D. J.; Oh, S.-H. Three-Dimensional Plasmonic Nanofocusing. *Nano Lett.* **2010**, *10*, 1369–1373.
9. Treutlein, P.; Hunger, D.; Camerer, S.; Hänsch, T. W.; Reichel, J. Bose–Einstein Condensate Coupled to a Nanomechanical Resonator on an Atom Chip. *Phys. Rev. Lett.* **2007**, *99*, 140403–140406.
10. Bleszynski-Jayich, A. C.; Shanks, W. E.; Peaudecerf, B.; Ginossar, E.; von Oppen, F.; Glazman, L.; Harris, J. G. E. Persistent Currents in Normal Metal Rings. *Science* **2009**, *326*, 272–275.
11. Tseng, S. C.; Peng, W. Y.; Hsieh, Y. F.; Lee, P. J.; Lai, W. L. Electron Beam Lithography on Cylindrical Roller. *Microelectron. Eng.* **2010**, *87*, 943–946.
12. Ahn, S. H.; Guo, L. J. High-Speed Roll-to-Roll Nanoimprint Lithography on Flexible Plastic Substrates. *Adv. Mater.* **2008**, *20*, 2044–2049.
13. Ge, H. X.; Li, Z. W.; Gu, Y. N.; Wang, L.; Wu, W.; Xia, Q. F.; Yuan, C. S.; Chen, Y.; Cui, B.; Williams, R. S. Hybrid Nanoimprint-Soft Lithography with Sub-15 nm Resolution. *Nano Lett.* **2009**, *9*, 2306–2310.
14. Linden, J.; Thanner, C.; Schaaf, B.; Wolff, S.; Lägel, B.; Oesterschulze, E. Spray Coating of PMMA for Pattern Transfer *via* Electron Beam Lithography on Surfaces with High Topography. *Microelectron. Eng.* **2011**, *88*, 2030–2032.
15. Yamazaki, K.; Yamaguchi, H. Electron Beam Lithography on Vertical Side Faces of Micrometer-Order Si Block. *J. Vac. Sci. Technol. B* **2012**, *30*, 041601–041606.
16. Peterson, I. R. Langmuir-Blodgett Electron-Beam Resists. *IEE Proc.-I: Solid-State Electron Devices I* **1983**, *130*, 252–255.
17. Carr, D. W.; Lercel, M. J.; Whelan, C. S.; Craighead, H. G.; Seshadri, K.; Allara, D. L. High-Selectivity Pattern Transfer Processes for Self-Assembled Monolayer Electron Beam Resists. *J. Vac. Sci. Technol. A* **1997**, *15*, 1446–1450.
18. Gölzhäuser, A.; Geyer, W.; Stadler, V.; Eck, W.; Grunze, M.; Edinger, K.; Weimann, T.; Hinze, P. Nanoscale Patterning of Self-Assembled Monolayers with Electrons. *J. Vac. Sci. Technol. B* **2000**, *18*, 3414–3418.
19. Pedersen, R. H.; Hamzah, M.; Thoms, S.; Roach, P.; Alexander, M. R.; Gadegaard, N. Electron Beam Lithography Using Plasma Polymerized Hexane as Resist. *Microelectron. Eng.* **2010**, *87*, 1112–1114.
20. Kelkar, P. S.; Beauvais, J.; Lavallée, E.; Drouin, D.; Cloutier, M.; Turcotte, D.; Yang, P.; Mun, L. K.; Legario, R.; Awad, Y.; *et al*. Nano Patterning on Optical Fiber and Laser Diode Facet with Dry Resist. *J. Vac. Sci. Technol. A* **2004**, *22*, 743–746.
21. Lavallée, E.; Beauvais, J.; Drouin, D.; Kelkar, P.; Yang, P.; Turcotte, D.; Cloutier, M.; Legario, R. Evaporated Electron Beam Lithography Resist for Non-Planar Surfaces. In *Microprocesses and Nanotechnology Conference 2003. Digest of Papers*; **2003**; pp 152–153.
22. Awad, Y.; Lavallée, E.; Lau, K. M.; Beauvais, J.; Drouin, D.; Cloutier, M.; Turcotte, D.; Yang, P.; Kelkar, P. Arrays of Holes Fabricated by Electron-Beam Lithography Combined with Image Reversal Process Using Nickel Pulse Reversal Plating. *J. Vac. Sci. Technol. A* **2004**, *22*, 1040–1043.
23. King, G. M.; Schürmann, G.; Branton, D.; Golovchenko, J. A. Nanometer Patterning with Ice. *Nano Lett.* **2005**, *5*, 1157–1160.
24. Gardener, J. A.; Golovchenko, J. A. Ice-Assisted Electron Beam Lithography of Graphene. *Nanotechnology* **2012**, *23*, 185302–185307.
25. Bahlke, M. E.; Mendoza, H. A.; Ashall, D. T.; Yin, A. S.; Baldo, M. A. Dry Lithography of Large-Area, Thin-Film Organic Semiconductors Using Frozen CO_2 Resists. *Adv. Mater.* **2012**, *24*, 6136–6140.
26. Muray, A.; Isaacson, M.; Adesida, I. AlF_3—A New Very High Resolution Electron Beam Resist. *Appl. Phys. Lett.* **1984**, *45*, 589–591.
27. Macaulay, J. M.; Allen, R. M.; Brown, L. M.; Berger, S. D. Nanofabrication Using Inorganic Resists. *Microelectron. Eng.* **1989**, *9*, 557–560.
28. Pennelli, G.; Totaro, M.; Piotto, M. Selective Doping of Silicon Nanowires by Means of Electron Beam Stimulated Oxide Etching. *Nano Lett.* **2012**, *12*, 1096–1101.
29. Ma, S.; Con, C.; Yavuz, M.; Cui, B. Polystyrene Negative Resist for High-Resolution Electron Beam Lithography. *Nanoscale Res. Lett.* **2011**, *6*, 446–451.
30. Con, C.; Dey, R.; Ferguson, M.; Zhang, J.; Mansour, R.; Yavuz, M.; Cui, B. High Molecular Weight Polystyrene as Very Sensitive Electron Beam Resist. *Microelectron. Eng.* **2012**, *98*, 254–257.
31. Con, C.; Arwa, S. A.; Yavuz, M.; Cui, B. Dry Thermal Development of Negative Electron Beam Resist Polystyrene. *Adv. Nano Res.* **2013**, *1*, 105–109.
32. Gerbedoen, J.-C.; Aliane, A.; Giguère, A.; Drouin, D.; Ares, R.; Aimez, V. All Evaporation Submicron Lift-off Lithography Process with Negative E-Beam QSR-5 Resist. *Microelectron. Eng.* **2013**, *103*, 123–125.
33. Beyler, C. L.; Hirschler, M. M. Chapter 7: Thermal Decomposition of Polymers. In *SFPE Handbook of Fire Protection Engineering*; National Fire Protection Association Quincy: Bethesda, MD, 1988.
34. Abbas, A. S.; Yavuz, M.; Cui, B. Polycarbonate Electron Beam Resist Using Solvent Developer. *Microelectron. Eng.* **2014**, *113*, 140–142.
35. Kashyap, R. *Fiber Bragg Gratings*, 2nd ed.; Academic Press: San Diego, CA, 2010; pp XV–XVI.
36. Xu, Q. B.; Bao, J. M.; Rioux, R. M.; Perez-Castillejos, R.; Capasso, F.; Whitesides, G. M. Fabrication of Large-Area Patterned Nanostructures for Optical Applications by Nanoskiving. *Nano Lett.* **2007**, *7*, 2800–2805.
37. Paul, K. E.; Zhu, C.; Love, J. C.; Whitesides, G. M. Fabrication of Mid-Infrared Frequency-Selective Surfaces by Soft Lithography. *Appl. Opt.* **2001**, *40*, 4557–4561.

38. Kneipp, K.; Kneipp, H.; Itzkan, I.; Dasari, R. R.; Feld, M. S. Surface-Enhanced Raman Scattering and Biophysics. *J. Phys.: Condens. Matter* **2002**, *14*, R597–R624.
39. Muskens, O. L.; Diedenhofen, S. L.; Kaas, B. C.; Algra, R. E.; Bakkers, E. P. A. M.; Rivas, J. G.; Lagendijk, A. Large Photonic Strength of Highly Tunable Resonant Nanowire Materials. *Nano Lett.* **2009**, *9*, 930–934.
40. Kang, S.; Joe, H. E.; Kim, J.; Jeong, Y.; Min, B. K.; Oh, K. Subwavelength Plasmonic Lens Patterned on a Composite Optical Fiber Facet for Quasi-One-Dimensional Bessel Beam Generation. *Appl. Phys. Lett.* **2011**, *98*, 241103–241105.
41. Liu, Y. X.; Xu, H.; Stief, F.; Zhitenev, N.; Yu, M. Far-Field Superfocusing with an Optical Fiber Based Surface Plasmonic Lens Made of Nanoscale Concentric Annular Slits. *Opt. Express* **2011**, *19*, 20233–20243.
42. Wang, H. X.; Zhou, W.; Cui, Y.; Wang, G. H.; Shum, P. P. Focused Ion Beam Nanoscale Patterned Transmission-Enhanced Fiber-Optic Tips. *J. Nanosci. Nanotechnol.* **2013**, *13*, 4581–4586.
43. Jia, P. P.; Jiang, H.; Sabarinathan, J.; Yang, J. Plasmonic Nanohole Array Sensors Fabricated by Template Transfer with Improved Optical Performance. *Nanotechnology* **2013**, *24*, 195501–195507.
44. Zhang, J.; Shokouhi, B.; Cui, B. Tilted Nanostructure Fabrication by Electron Beam Lithography. *J. Vac. Sci. Technol. B* **2012**, *30*, 06F302.
45. Dey, R. K.; Cui B. Electron Beam Lithography with *in-Situ* Feedback Using Self-Developing Resist, *Nanoscale Res. Lett.*, in press.
46. Burek, M. J.; de Leon, N. P.; Shields, B. J.; Hausmann, B. J. M.; Chu, Y.; Quan, Q.; Zibrov, A. S.; Park, H.; Lukin, M. D.; Lončar, M. Free-Standing Mechanical and Photonic Nanostructures in Single-Crystal Diamond. *Nano Lett.* **2012**, *12*, 6084–6089.
47. Takahashi, S.; Suzuki, K.; Okano, M.; Imada, M.; Nakamori, T.; Ota, Y.; Ishizaki, K.; Noda, S. Direct Creation of Three-Dimensional Photonic Crystals by a Top-Down Approach. *Nat. Mater.* **2009**, *8*, 721–725.
48. Dey, R. K.; Cui, B. Effect of Molecular Weight Distribution on E-Beam Exposure Properties of Polystyrene. *Nanotechnology* **2013**, *24*, 245302–245306.